Transient photoresponse and incident power dependence of high-efficiency germanium quantum dot photodetectors

Pei Liu,[1] S. Cosentino,[2,3] Son T. Le,[1] S. Lee,[2] D. Paine,[2] A. Zaslavsky,[2] D. Pacifici,[2,a)] S. Mirabella,[3] M. Miritello,[3] I. Crupi,[3] and A. Terrasi[3]

[1]*Physics Department, Brown University, Providence, Rhode Island 02912, USA*
[2]*School of Engineering, Brown University, Providence, Rhode Island 02912, USA*
[3]*MATIS-IMM-CNR and Dipartimento di Fisica ed Astronomia, Università di Catania, Catania I-95123, Italy*

(Received 24 August 2012; accepted 25 September 2012; published online 19 October 2012)

We report a systematic study of time-resolved and power-dependent photoresponse in high-efficiency germanium quantum dot photodetectors (Ge-QD PDs), with internal quantum efficiencies greater than 100% over a broad wavelength, reverse bias, and incident power range. Turn-on and turn-off response times (τ_{on} and τ_{off}) are shown to depend on series resistance, bias, optical power, and thickness (W_{QD}) of the Ge-QD layer, with measured τ_{off} values down to $\sim$40 ns. Two different photoconduction regimes are observed at low and high reverse bias, with a transition around -3 V. A transient current overshoot phenomenon is also observed, which depends on bias and illumination power. © *2012 American Institute of Physics*. [http://dx.doi.org/10.1063/1.4759252]

I. INTRODUCTION

Group IV semiconductor quantum dots (QDs) have been extensively studied for optoelectronic and photovoltaic applications to improve the performance of devices such as lasers, photodetectors (PDs), and solar cells.[1–7] By shrinking the size of bulk materials down to the nanoscale to form QDs, indirect bandgap group-IV semiconductors can be used as efficient light absorbing or emitting materials. For example, the incorporation of Si QDs has been shown to successfully increase PD efficiency up to 200% in the visible range.[8,9] Compared to Si QDs, Ge QDs offer some advantages: they can be easily embedded in SiO_2 at lower temperatures[10,11] and have higher absorption coefficients due to localized defect states at the Ge/SiO_2 interface.[12] We have recently reported on high-efficiency PDs based on a metal-insulator-semiconductor (MIS) structure, with the insulating layer consisting of a dense array of $\sim$2 to 3 nm diameter amorphous Ge-QDs embedded in a silica matrix, of total thickness $W_{QD} = 230$ nm. Internal quantum efficiency (IQE) as high as 700% in the 500–1000 nm wavelength range, as well as peak responsivity approaching 4 A/W, were measured at -10 V reverse bias in the as-prepared samples, without the need for additional high-temperature annealing steps.[11] In this paper, we present a systematic study on the response time and responsivity as functions of illumination power, reverse bias, and active QD layer thickness W_{QD} in the 60–230 nm range. We demonstrate turn-off response times (τ_{off}) down to $\sim$40 ns as well as a general $\tau_{off} \sim W_{QD}^2$ dependence, characteristic of carrier diffusive hopping between QDs within the oxide matrix.

II. DEVICE FABRICATION AND CHARACTERIZATION

A 230 nm-thick oxide layer containing amorphous Ge quantum dots was fabricated by rf-magnetron co-sputtering deposition on an *n*-type Si substrate held at 400 °C using SiO_2 and Ge targets.[11] Thinner active layers were then obtained by etching the original as-deposited films in an HF etchant solution for SiO_2. Reflectance and ellipsometric measurements were performed to determine the final thickness W_{QD} in the 60–230 nm range. A transparent top metal contact was then realized by sputter-depositing indium-zinc-oxide (IZO) conductive films on all samples. The active area of our devices was 4×4 mm^2. A schematic picture of our devices is shown in the inset of Fig. 1, and additional fabrication details have been published elsewhere.[11]

In order to further characterize these devices, both optical and electrical measurements were carried out. Specular reflectance as well as internal and external quantum efficiencies were measured using a QEX10 quantum efficiency measurement system (from PV measurement) calibrated using reference cells over the $\lambda = 400$–1100 nm wavelength range. The $I(V)$ measurements were carried out using an Agilent 4155C parameter analyzer. Subsequently, the transient photoresponse of Ge-QD PDs was studied by illuminating the device (held at constant reverse bias V) with a modulated diode laser (either by a mechanical chopper or through direct digital modulation of the laser) at $\lambda = 670$ nm. The laser beam was focused on a $\sim$3 mm diameter spot. The photogenerated current was then measured from an oscilloscope by recording the voltage drop across a resistor in series with the PD.

III. RESULTS AND DISCUSSION

Figure 1(a) shows the rectifying current-voltage $I(V)$ characteristics of a Ge-QD PD device with $W_{QD} = 230$ nm, as measured in the dark and under illumination using a diode laser at $\lambda = 670$ nm, at various incident optical power P_{opt}. While there is no significant photoresponse in forward bias, the reverse bias current is strongly enhanced by optical illumination, with the reverse current increasing by a factor $\sim 10^3$. For a given incident power, two distinct regimes can be clearly observed in the photocurrent response vs. reverse

a)Author to whom correspondence should be addressed. Electronic mail: Domenico_Pacifici@brown.edu.

 © 2012 American Institute of Physics

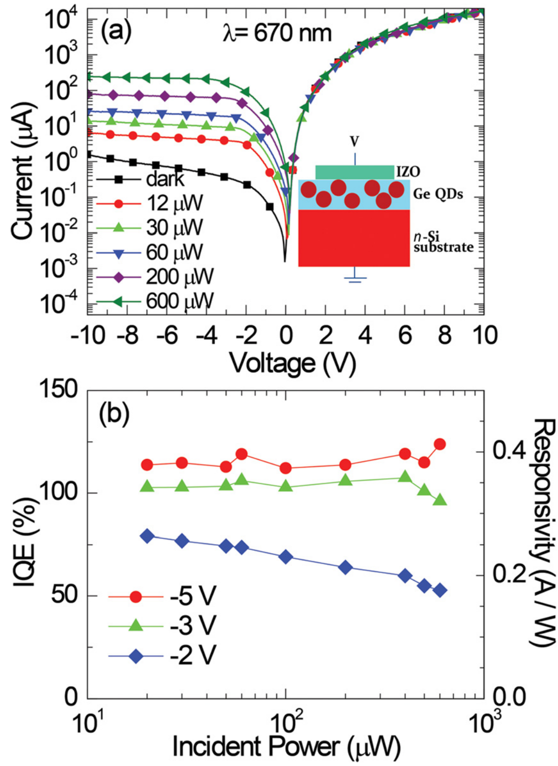

FIG. 1. (a) Current-voltage $I(V)$ characteristics for Ge-QD PD with $W_{QD} = 230$ nm at different illumination powers; the inset shows a schematic of the device; (b) IQE (left axis) and responsivity (right axis) vs. incident power P_{opt} measured at various reverse bias.

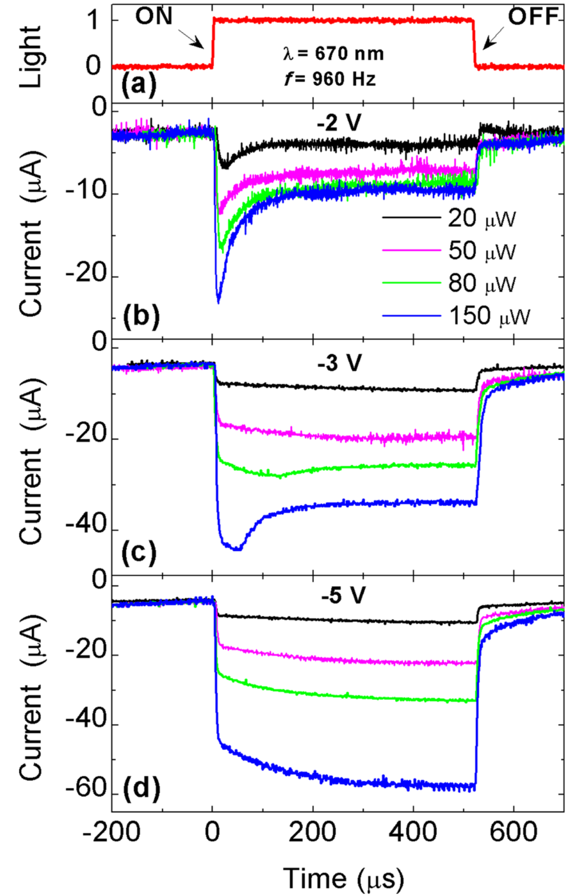

FIG. 2. Transient photoresponse curves for Ge-QD PD with $W_{QD} = 230$ nm under illumination using a $\lambda = 670$ nm laser beam modulated by a mechanical chopper at $f = 960$ Hz: (a) a representative illumination square waveform; transient photocurrent response under (b) −2 V, (c) −3 V, and (d) −5 V bias. The photocurrent signal was obtained by measuring the voltage drop across a load resistor ($R = 10$ kΩ) recorded using an oscilloscope.

bias plot: a "low bias" regime for $-3 < V < 0$ V where the photogenerated current changes drastically with bias, and a "high bias" regime for $V < -3$ V, where the photocurrent does not change significantly with increasing V. Figure 1(b) reports the internal quantum efficiency (IQE, left axis, defined as the number of photogenerated carriers divided by the number of absorbed photons) and spectral responsivity (R_{sp}, right axis, defined as the ratio between the photogenerated current and the incident optical power) as functions of incident optical power for several values of reverse bias as calculated from Fig. 1(a) using the following equations:

$$IQE = \frac{hc}{\lambda q(1-r)} R_{sp}, \quad \text{where } R_{sp} = \frac{(I_{light} - I_{dark})}{P_{opt}}, \tag{1}$$

where I_{light} and I_{dark} are the currents measured under illumination and in the dark, respectively, P_{opt} is the optical power incident on the device, as measured by a calibrated silicon PD, $r \sim 47\%$ is the specular reflectance of the three-layer system (IZO/W_{QD}/Si) measured under normal incidence illumination at $\lambda = 670$ nm, q is the elementary charge, h and c are Planck's constant and the speed of light in vacuum, respectively. As proposed in Ref. 11, the high IQE observed in Fig. 1(b) can be explained as the result of preferential trapping of photogenerated holes in the QD layer, which causes an increase in the flow of electrons from the IZO contact to maintain charge neutrality in the film. Higher applied bias leads to increased injection and trapping of holes, with consequent enhancement of photoconductive gain and internal quantum efficiency. Figure 1(b) also shows that both IQE and responsivity remain roughly constant over the entire $P_{opt} = 10$–$600\,\mu$W range for high applied reverse bias ($V = -3$ V and above), whereas at $V = -2$ V the IQE decreases as P_{opt} increases.

Figure 2 shows the time response measurement under a modulated incident light beam at $\lambda = 670$ nm on the same device. Figure 2(a) shows the modulation of the incoming light beam with an optical modulation frequency of 960 Hz. The measurements were done at three different values of reverse bias ($V = -2$, -3, and -5 V, Figs. 2(b)–2(d), respectively) for various illumination powers, using a 10 kΩ series resistor. In all cases, a rapid initial rise of the photocurrent magnitude is observed as the light is switched on. Specifically, at $V = -2$ V, the photocurrent shows a fast turn-on-time overshoot, followed by a slower transient to a steady-state value, which depends on P_{opt}. The initial photocurrent overshoot level depends on the incident power and can be attributed to a fast photo-absorption, followed by carrier injection and hopping transport of electrons and holes through the QD layer. The slower transient behavior that follows the overshoot suggests that charging in the QDs is followed by electric field redistribution inside the QD-containing film. Indeed, as a result of localized charging of QDs near the interface, the average field across the remaining QD layer will decrease to ensure that the total applied voltage across

the entire film remains constant. As a consequence of the reduced average electric field, a reduced drift current will follow, thus explaining the lower steady state current values after the initial overshoot. At $V = -3$ V, the overshoot is not observed if the incident power is sufficiently low. But at higher powers, the larger trapped charge density will lead to an increased voltage drop across the device, thus causing a photocurrent overshoot. A similar photocurrent overshoot was previously reported in a different system, consisting of GaAs/AlGaAs superlattice-based infrared PDs operating at low temperature, and was attributed to charging of the first few quantum wells with subsequent reduction of the electric field in the rest of the superlattice.[13]

Another important aspect to consider when describing the device transient behavior is the possible voltage drop that can occur across the series resistor itself. For example, at $V = -3$ V and $P_{opt} = 150\ \mu$W, the measured peak current is $-44\ \mu$A, corresponding to a voltage drop of -0.44 V across the 10 kΩ resistor, which means that a voltage of -2.56 V (instead of the full -3 V) is actually applied across the QD layer. Under these conditions, the device is effectively operating in the low bias regime, where the overshoot can again take place. At even higher applied bias (for example, -5 V, Fig. 2(d)), the current overshoot is no longer observed. Indeed, after the laser is turned on, although the photocurrent increases with time, the small voltage drop across the resistor does not generate a significant change in current, since the device is operated in the "high" bias regime characterized by a saturated *I(V)* response. Therefore, the photocurrent reaches a steady state value, which remains roughly constant as a function of time.

From the time-resolved measurements reported in Figs. 2(b)–2(d), the steady state photocurrent vs. power dependence can be extracted, as reported in Fig. 3(a). At -2 V, the steady-state photocurrent strongly saturates as the incident power P_{opt} is increased, showing a sublinear behavior, which is also responsible for the decrease in responsivity observed in Fig. 1(b) (at -2 V); at higher reverse bias (-3 and -5 V), the steady-state photocurrent shows a nearly linear trend with respect to P_{opt}. This is consistent with the results previously reported in Fig. 1(b), where at -3 and -5 V, the responsivity remains roughly constant with increasing P_{opt}. Therefore, the different IQE vs. incident power dependence under low and high reverse bias conditions can be understood as the result of two different conduction regimes, corresponding to the "low" and "high" bias regimes in the *I(V)* characteristics as noted in Fig. 1(a).

We would like to notice here that the responsivity values extracted from the steady-state portion of the transient photocurrent response curves are somewhat lower than the responsivity extracted from continuous wave (CW) measurements. Indeed, as we will see in the following, the device response time can affect the frequency dependence of its responsivity.

For this reason, rise (τ_{on}) and decay (τ_{off}) times of a PD are critical parameters. The τ_{on} consists of an intrinsic, optically induced turn-on time (directly linked to the optical excitation rate of electron-hole pairs in the QDs and in the silicon substrate) together with a contribution from the characteristic *RC* time constant. To quantify the effects of *RC* and optical excitation rate on τ_{on}, we carried out the experiment under several different load resistances *R* and illumination powers. We define τ_{on} as the time it takes for the device to reach $(1 - 1/e)$ or ~63% of the maximum photocurrent of the fast initial increase. The photocurrent rise time data for $V = -2$ V, normalized to the peak photocurrent, are shown in the inset of Fig. 3(b). The results are summarized in Fig. 3(b), where we plot τ_{on} vs. *R* for $V = -2$ V bias, and at two different P_{opt} values. As expected, τ_{on} decreases with *R* for a given P_{opt} due to a smaller *RC* time constant, with a minimum τ_{on} falling in the 1–2 μs range, fast compared to other reported QD-based PDs.[14–16] Figure 3(b) also shows that, for a given series resistance, faster turn-on times can be achieved by increasing the incident optical power, due to a higher excitation rate. The bias dependence of the PD turn-

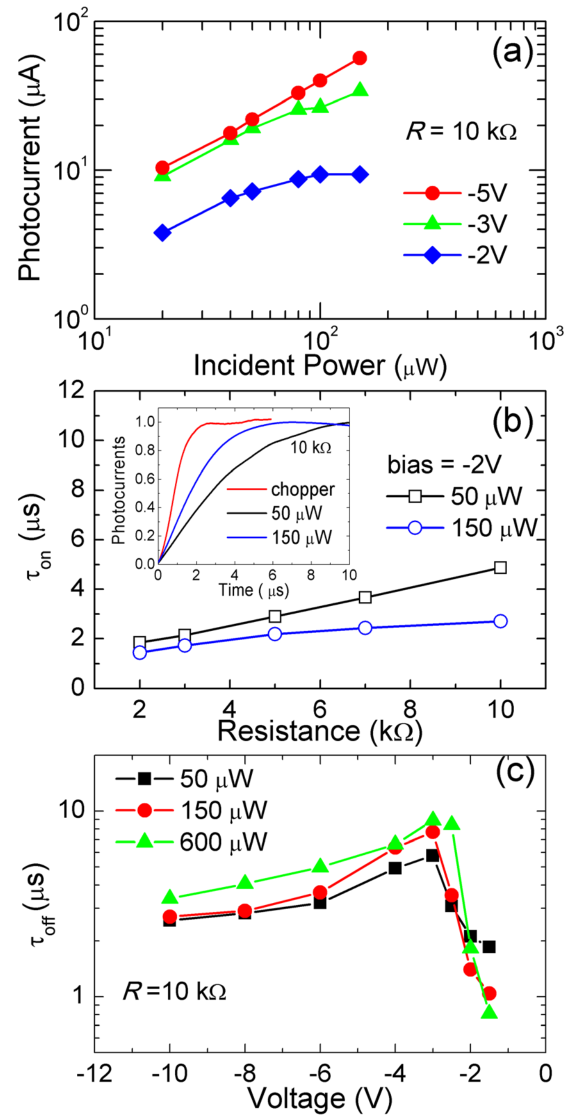

FIG. 3. (a) Steady state photocurrent as extracted from Fig. 2 vs. incident power, at different bias; (b) measured turn-on time τ_{on} vs. load resistor *R* at -2 V bias, and for different incident powers for Ge-QD PD with $W_{QD} = 230$ nm. The inset shows the normalized photocurrent time-resolved curves for $R = 10$ kΩ load resistor vs. illumination power. The red line represents the system response obtained by measuring the modulated laser beam using a commercial Si photodiode; (c) measured turn-off time τ_{off} vs. bias voltage as a function of incident pump power for the same sample.

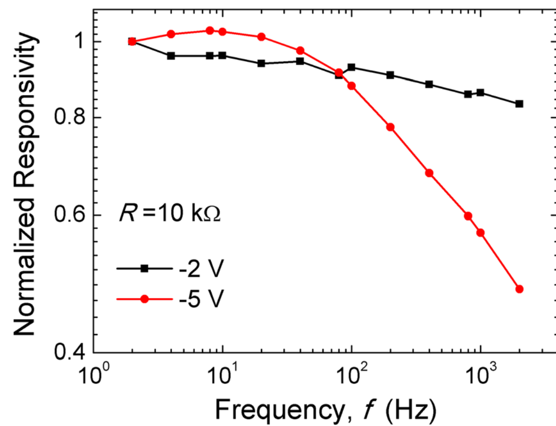

FIG. 4. Normalized responsivity vs. frequency f at -2 V and -5 V bias for Ge-QD PDs with $W_{QD} = 230$ nm. The incident power is 8.2 μW and $R = 10$ kΩ.

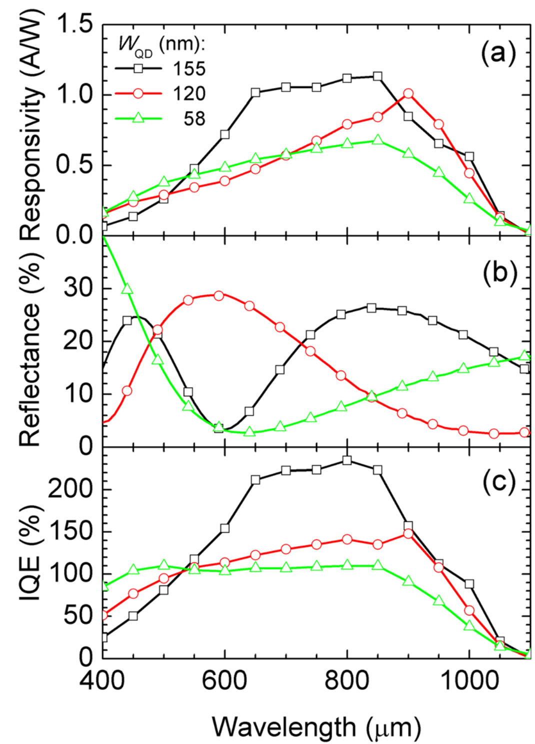

FIG. 5. (a) Spectral responsivity; (b) reflectance; (c) IQE for devices with varying active thicknesses W_{QD} at -2 V bias.

off time (τ_{off}) is reported in Fig. 3(c), where two distinct regimes for τ_{off} as a function of applied bias are experimentally observed. The two different regimes can be correlated with the two different conduction regimes discussed above in Fig. 1(a), namely the "low" and the "high" bias regimes, corresponding respectively to drift-limited (faster) and diffusion-limited (slower) carrier conduction through the QD layer, with a transition between the two regimes observed again at $V \sim -3$ V. In order to further confirm this time response behavior, we measured responsivity as a function of laser modulation frequency f, as shown in Fig. 4. Our measurements show that the responsivity decreases more drastically as a function of frequency f at -5 V, compared to -2 V. This is consistent with the different response times observed at -2 V and -5 V, as shown in Fig. 3(c).

Based on the presented results, assuming one of the main delays comes from the transit time due to the percolative hopping of conduction electrons through the QD layer—which to first approximation is proportional to W_{QD}^2—faster response times can be achieved by reducing the QD layer thickness. We therefore fabricated devices with different QD layer thicknesses as discussed in Section II. The measured responsivity (at -2 V reverse bias), reflectance, and IQE from some representative devices with thinner active layer are reported in Fig. 5 for various W_{QD}. By fitting the reflectance curves in Fig. 5(b) using a multiple reflection model for the two-layer system that takes into account the optical constants of the various dielectric layers, we were able to extract the QD layer thickness W_{QD}. The error range for these W_{QD} values, arising from the estimated error in the Ge concentration measurement in these Ge-rich layers obtained by Rutherford backscattering spectrometry (RBS, not shown), is reported as horizontal error bars in Fig. 6(b). From Fig. 5(c), we observe that reducing W_{QD} only slightly reduces the internal quantum efficiencies of these devices. Interestingly, for the thinnest device ($W_{QD} \sim 60$ nm), the IQE is roughly constant to $\sim$100% over a wide wavelength range, from 400–850 nm. On the other hand, the response time (τ_{off}) of these devices, shown in Fig. 6, decreases quickly with W_{QD}. For example, reducing W_{QD} down to $\sim$60 nm reduces τ_{off} to $\sim$40 ns, as shown in the inset of Fig. 6(b), at the cost of a slightly lower responsivity (but

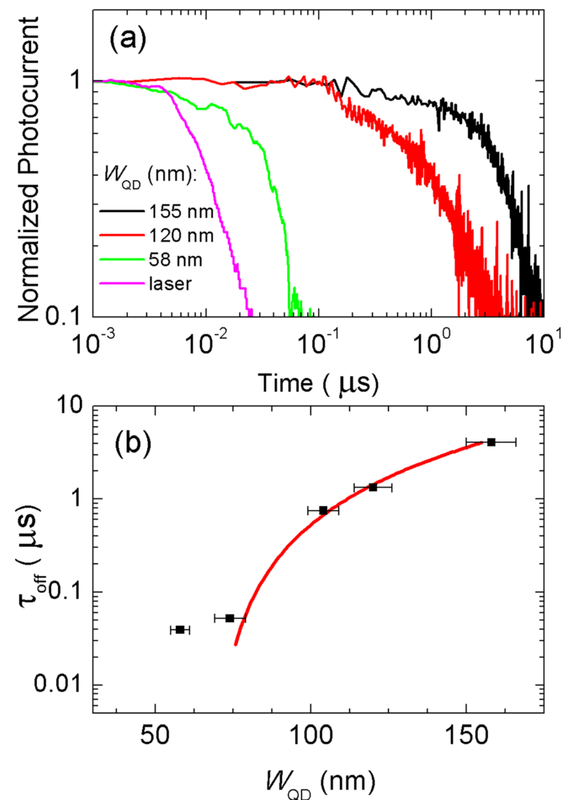

FIG. 6. (a) Time-resolved normalized photocurrent response measured at -2 V bias and 2 mW incident power (using a load resistor with $R = 50\ \Omega$); (b) measured τ_{off} vs. W_{QD} (solid squares) and fit of the experimental data showing a quadratic dependence (red line).

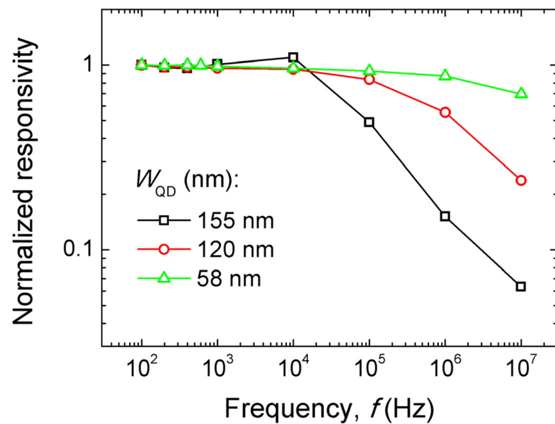

FIG. 7. Normalized responsivity vs. frequency f for devices with $W_{QD} = 155$ nm, 120 nm and 58 nm. For this set of measurements, $R = 50\ \Omega$, $P_{opt} = 1$ mW, and $V = -2$ V.

still above 0.5 A/W). In order to verify our proposed carrier hopping mechanism, the red curve in Fig. 6(b) shows a quadratic fit of the measured response times with respect to W_{QD}. As is seen from the figure, the fit is reasonably consistent with the measured data except at the lowest W_{QD}, where the deviation can be attributed to parasitic capacitance. Indeed, the measured capacitance for the thinnest device is about 260 pF. Given that we are using a load resistor with $R = 50\ \Omega$, a lower bound to the circuit RC constant is of the order of $\sim$10 ns, i.e., the same order of magnitude of the fastest measured response time. This suggests that an even faster response time can be achieved by reducing the parasitic series resistance and capacitance, the device area, and decreasing W_{QD} even further. There may also be room for improvement in the response time by optimizing the Ge QD size and distribution in the active layer.

Finally, we would like to point out that the bandwidth of a photodetector is closely related to the response speed. By reducing the active QDs layer thicknesses, we are able to achieve faster response time as just shown above, and thus we would expect larger bandwidths as well. Therefore, we performed responsivity measurements over a wide modulation frequency range of illumination for these devices, as reported in Fig. 7. To reduce the RC time delay, we used an $R = 50\ \Omega$ resistor in the measurement circuit. As we have seen in the figure, the responsivity of the device generally decreases as f increases, but while the responsivity of the $W_{QD} = 155$ nm device begins to fall off already after $\sim 10^4$ Hz, for thinner W_{QD} devices the roll-off can be pushed to higher frequencies as the result of the faster rise and decay times. Moreover, for the thinner device with $W_{QD} = 58$ nm, the responsivity is roughly constant up to operating frequencies of $\sim 10^7$ Hz.

IV. CONCLUSION

In summary, in this paper, we report on responsivity and response time measurements of high internal quantum efficiency Ge-QD photodetectors as functions of active layer thickness, illumination power, and applied reverse bias. We reveal two distinct operating regimes depending on applied bias that can be attributed to drift- (low bias) and diffusion-limited (high bias) conduction mechanisms, respectively. By measuring the photodetector response time as a function of oxide layer thickness, we find a $\tau_{off} \sim W_{QD}^2$ dependence, which experimentally supports the hypothesis that carrier transport in this system occurs mainly by hopping through a percolative network of quantum dots. We show that photodetectors based on germanium quantum dots as the active medium with active layers as thin as $\sim$60 nm can achieve high internal quantum efficiencies (>100%, roughly constant over a broad wavelength range between 400 and 1100 nm), response times as fast as $\sim$40 ns, at operating voltages of only -2 V. These advantages together with the ease of fabrication and low temperature processing, make germanium quantum dots a promising candidate for CMOS-compatible, integrated photodetector applications including fast, low power consumption cameras, and integrated biochemical sensors.

ACKNOWLEDGMENTS

The authors thank P. Flanigan for useful discussions. This work was performed in part at the Brown Microelectronics Facility, and in part at the MATIS-IMM-CNR (Catania, Italy). Funding from the National Science Foundation (Grant Nos. ECCS-1068895, DMR-1203186, and DMR-0804915) is gratefully acknowledged. One of the authors (S.C.) acknowledges support from a scholarship grant awarded by the Blanceflor Boncompagni-Ludovisi Foundation.

[1]K. Brunner, Rep. Prog. Phys. **65**, 27 (2002).
[2]U. Kortshagen, R. Anthony, R. Gresback, Z. Holman, R. Ligman, C. Liu, L. Mangolini, and S. A. Campbell, Pure Appl. Chem. **80**, 1901 (2008).
[3]O. P. Pchelyakov, A. I. Nikiforov, B. Z. Olshanetsky, S. A. Teys, A. I. Yakimov, and S. I. Chikichev, J. Phys. Chem. Solids **69**, 669 (2008).
[4]K. L. Wang, D. Cha, J. Liu, and C. Chen, Proc. IEEE **95**, 1866 (2007).
[5]L. Pavesi, L. Dal Negro, C. Mazzoleni, G. Franzò, and F. Priolo, Nature **408**, 440 (2000).
[6]A. M. Kechiantz, L. M. Kocharyan, and H. M. Kechiyants, Nanotechnology **18**, 405401 (2007).
[7]B. C. Hsu, S. T. Chang, T. C. Chen, P. S. Kuo, P. S. Chen, Z. Pei, and C. W. Liu, IEEE Electron Dev. Lett. **24**, 318 (2003).
[8]J. M. Shieh, Y. F. Lai, W. X. Ni, H. C. Kuo, C. Y. Fang, J. Y. Huang, and C. L. Pan, Appl. Phys. Lett. **90**, 051105 (2007).
[9]J. M. Shieh, W. C. Yu, J. Y. Huang, C. K. Wang, B. T. Dai, H. Y. Jhan, C. W. Hsu, H. C. Kuo, F. L. Yang, and C. L. Pan, Appl. Phys. Lett. **94**, 241108 (2009).
[10]B. Zhang, S. Shrestha, M. A. Green, and G. Conibeer, Appl. Phys. Lett. **96**, 261901 (2010).
[11]S. Cosentino, Pei Liu, Son T. Le, S. Lee, D. Paine, A. Zaslavsky, S. Mirabella, M. Miritello, I. Crupi, A. Terrasi, and D. Pacifici, Appl. Phys. Lett. **98**, 221107 (2011).
[12]S. Cosentino, S. Mirabella, M. Miritello, G. Nicotra, R. Lo Savio, F. Simone, C. Spinella, and A. Terrasi, Nanoscale Res. Lett. **6**, 135 (2011).
[13]V. Letov, M. Ershov, S. G. Matsik, A. G. U. Perera, H. C. Liu, Z. R. Wasilewski, and M. Buchanan, Appl. Phys. Lett. **79**, 2094 (2001).
[14]M. Martens, J. Schlegel, P. Vogt, F. Brunner, R. Lossy, J. Würfl, M. Weyers, and M. Kneissl, Appl. Phys. Lett. **98**, 211114 (2011).
[15]L. Chu, A. Zrenner, D. Bougeard, M. Bichler, and G. Abstreiter, Phys. E **13**, 301 (2002).
[16]S. H. Im, J. A. Chang, Sung Woo Kim, Sang-Wook Kim, and S. Seok, Org. Electron. **11**, 696 (2010).